THE JOURNAL OF PHYSICAL CHEMISTRY Letters

pubs.acs.org/JPCL

Ab Initio Molecular Dynamics Study of an Aqueous Solution of $[Fe(bpy)_3](Cl)_2$ in the Low-Spin and in the High-Spin States

Latévi Max Lawson Daku* and Andreas Hauser

Département de Chimie Physique, Université de Genève, Quai E. Ansermet 30, CH-1211 Genève 4, Switzerland

ABSTRACT The mechanism of the photoinduced low-spin → high-spin spin crossover is actively being investigated in Fe(II) complexes in solution using ultrafast spectroscopies. These studies accurately inform on the reaction coordinate of the Fe(II) chromophore upon photoexcitation. However, they leave open questions regarding the role of the solvent. Here, we report the description from a fully ab initio molecular dynamics study of the structure of $[Fe(bpy)_3]^{2+}$ in water and of the organization of its solvation shell in the low-spin and the high-spin states. In particular, the low-spin → high-spin change of states is shown to be accompanied (i) by a 0.191 Å lengthening of the Fe−N bond, in agreement with experiment, and (ii) by an increased thermal fluctuation of the molecular edifice, which both result from the weakening of the Fe−N bond. Furthermore, our results suggest that about two water molecules are expelled from the first solvation shell of $[Fe(bpy)_3]^{2+}$, which consists of water molecules intercalated between the bpy ligands.

SECTION Dynamics, Clusters, Excited States

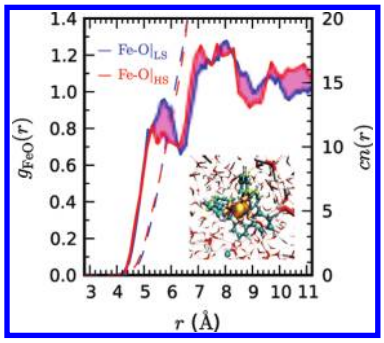

The electronic ground state of octahedral d^6 iron(II) complexes is either the low-spin (LS) $^1A_{1g}(t_{2g}^6)$ state or the high-spin (HS) $^5T_{2g}(t_{2g}^4e_g^2)$ state depending on the strength of the ligand field. Iron(II) complexes with a LS ground state and a close-lying HS state can exhibit spin crossover (SCO), namely, the entropy-driven thermal population of the HS state.[1] Iron(II)-tris(2,2′-bipyridine), $[Fe(bpy)_3]^{2+}$ (Chart 1), is a LS species. That is, the HS state is too high in energy to become thermally populated. However, as for Fe(II) SCO complexes, its HS state can be populated by photoexcitation, and the study of the kinetics of the HS → LS relaxation allowed the determination of its HS−LS energy difference in various crystalline environments.[2−6]

While the HS → LS intersystem crossing (ISC) is well-understood in terms of a nonadiabatic multiphonon relaxation process,[3] the mechanism of the photoinduced LS → HS crossover is the subject of current research. This mechanism was recently studied in Fe(II) SCO complexes in solution by the groups of McCusker and McGarvey using ultrafast time-resolved optical and vibrational spectroscopies.[7−12] It was similarly investigated in $[Fe(bpy)_3]^{2+}$ in aqueous solution by Chergui and co-workers, who also used ultrafast X-ray absorption spectroscopy to follow the structural changes undergone by the complex.[13−17] The emerging consensus is that, upon photoexcitation into the singlet metal-to-ligand charge-transfer (^{1}MLCT) manifold, a hot HS state is formed on a subpicosecond time scale and that vibrational cooling in the HS state occurs on a time scale of a few to one or several tens of picoseconds depending on the complex. The formation of

Chart 1. Drawing of $[Fe(bpy)_3]^{2+}$, Labels Used, And Definitions of the Bite Angle β and Torsion Angle γ

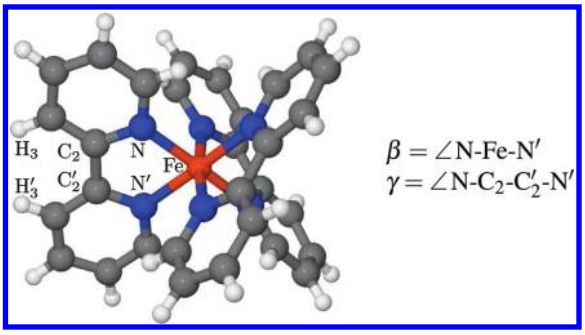

the hot HS state involves a first ISC step to the ^{3}MLCT manifold followed by a second step taking the molecule to the HS state. These studies accurately inform on the reaction coordinate of the Fe(II) chromophore upon photoexcitation.[21] However, they leave open the questions regarding the influence of the solvent on the early evolution of the complex, the involvement of the solvent in the dissipation of the excess energy, and the response of the solvation shell to the perturbation. Addressing these questions is, from both theoretical and experimental points of view, a challenging task to which we aim to contribute. Here, we report the description from a fully

Received Date: April 28, 2010
Accepted Date: May 23, 2010

DOI: 10.1021/jz100548m | *J. Phys. Chem. Lett.* **2010**, *1*, 1830–1835

ab initio molecular dynamics (AIMD) study of the structure of $[Fe(bpy)_3]^{2+}$ in aqueous solution and of the organization of its solvation shell in the LS and the HS states.

The AIMD simulations were performed at 300 K within the Car−Parrinello scheme,[22] as implemented in the CPMD code,[23,24] using the BLYP functional[25,26] (see the Supporting Information (SI) for the computational details). A large cubic simulation box of side 21 Å containing 1 $[Fe(bpy)_3]^{2+}$ complex, 2 Cl^- ions, and 298 water molecules was used.[27] The durations of the trajectories recorded in the LS and the HS state are 24.479 and 3.950 ps, respectively. Figure 1 shows a snapshot taken at the end of the HS trajectory, wherein the spin density is displayed. This one is centered on the Fe atom, and its shape shows that the spin polarization occurs in the Fe(3d) orbital levels of octahedral t_{2g} and e_g parentages, as expected.

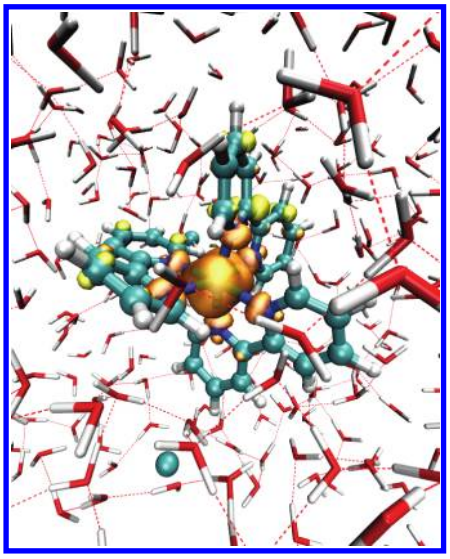

Figure 1. Snapshot from the HS trajectory showing $[Fe(bpy)_2]^{2+}$, a Cl^- ion, some water molecules with the H-bonding network, and the spin density.

In order to characterize the LS and HS structures of $[Fe(bpy)_3]^{2+}$ in solution, the thermal distributions of the average Fe−N and C_2-C_2' bond lengths and of the average values of the angles $\beta = \angle N-Fe-N'$ and $\gamma = \angle N-C_2N-C_2'-N'$ have been calculated in both spin states (see Chart 1 for the atom labeling). They are plotted in Figure 2, whose inspection shows that there is a ∼0.2 Å shift of the distribution of the Fe−N distance toward larger values upon the LS to HS change of states. The lengthening of the Fe−N bond results from the promotion of two electrons from the metallic nonbonding levels of t_{2g} parentage into the antibonding levels of e_g parentage. This weakening of the Fe−N bonds translates also into a broadening of the distribution, and the long tail of the HS distribution at large Fe−N distances can be ascribed to the increased anharmonicity of the Fe−N bond in the HS state. The distribution of the β angle gets shifted by ∼6° toward smaller values and broadens. One also notes a slight shift of the distribution of the C_2-C_2' distance toward larger values. The distribution of the γ angle in the LS state is centered at about 0 and is quite large owing to the fact that the deformations along this angular coordinate are associated with floppy modes.[4] In passing to the HS state, this distribution gets slightly shifted toward larger γ values and becomes even broader.

The thermal distributions could be satisfactorily fitted with Gaussian distribution functions (Figure 2). Table 1 summarizes the averages and standard deviations thus obtained for the geometric parameters. In the two spin states, and except for the angle γ, the average values derived from the AIMD

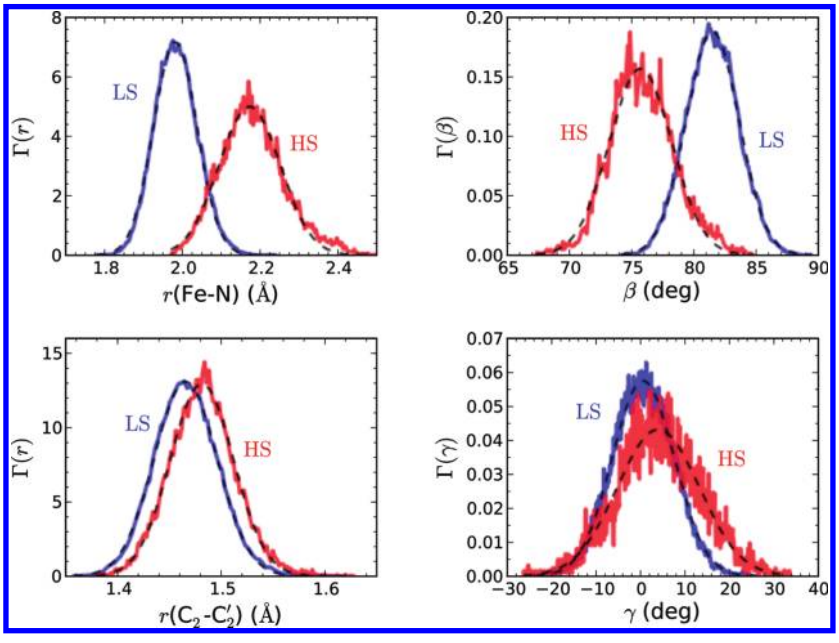

Figure 2. Thermal distributions in the LS and HS spin states of selected structural parameters of $[Fe(bpy)_3]^{2+}$ (solid lines). The fits of the data assuming Gaussian distributions are also shown (dashed lines).

DOI: 10.1021/jz100548m | J. Phys. Chem. Lett. 2010, 1, 1830–1835

simulations for the selected geometric parameters are close to their values in the optimized geometries of $[Fe(bpy)_3]^{2+}$ and, in the LS state, to those found in the crystal structure of the complex (Table 1). Given that the deformations along γ are associated with floppy modes, the noticeable differences between its values in Table 1 reflect the sensitivity of this angular coordinate to the environment. Hence, apart from small differences, which can be ascribed to environmental effects, the room-temperature (RT) solution structure of $[Fe(bpy)_3]^{2+}$ is similar in either spin state to its gas-phase geometry and, in the LS state, to its crystal structure. Thus, whatever the medium, the bpy ligand is nonplanar because of the steric repulsion between the adjacent H_3 and H'_3 atoms, and its geometry similarly evolves upon SCO (Table 1) so as to keep the Fe−bpy bonding optimal despite the lengthening of the Fe−N bond.

The Fe−N bond lengths of 1.982 and 2.173 Å predicted for the LS and HS aqueous structures agree very well with the experimental values obtained from the analysis of the LS static and HS transient EXAFS spectra of $[Fe(bpy)_3]^{2+}$ in water;[16] the differences are indeed within the experimental uncertainty of ∼0.01 Å, thus attesting for the high accuracy achieved for the description of the LS and HS geometries of $[Fe(bpy)_3]^{2+}$ in water. The standard deviations of the distributions increase upon SCO; this reflects the increased thermal fluctuations of the ligands.

The LS and HS average structures of aqueous $[Fe(bpy)_3]^{2+}$ have been calculated, and the root-mean-square fluctuations of the atomic positions about their average values have been calculated as well. Figure 3 gives views of the average structures showing 50 % probability ellipsoids associated with the thermal fluctuations of the atoms. Its inspection shows that in both spin states, the volumes of the ellipsoids, and hence the atomic disorders, increase upon moving away from the iron center, that is, the thermal fluctuations of the atoms logically increase with their exposure to the solvent. One also notes that the atomic displacements increase upon going from the LS to the HS state, which is a consequence of the weakening of the Fe−N bond. Finally, the superimposition of the LS and HS average structures (Figure 3) illustrates the previously discussed SCO-induced coordination geometry changes.

Table 1. Averages ($\bar{X}$) and Standard Deviations $\sigma(X)$ of Selected Structural Parameters Determined from the AIMD Simulations for $[Fe(bpy)_3]^{2+}$ in the LS and HS States along with Optimized and Available Experimental Values

		AIMD[a]		Opt.[a,b]	Cryst.[c]	EXAFS[d]
		$\bar{X}$	$\sigma(X)$			
Fe−N (Å)	LS	1.982	0.056	1.997	1.967	1.98
	HS	2.173	0.079	2.208		2.18
$C_2-C'_2$ (Å)	LS	1.466	0.030	1.468	1.471	
	HS	1.481	0.031	1.486		
β (deg)	LS	81.5	2.1	81.0	81.8	
	HS	75.7	2.5	75.0		
γ (deg)	LS	0.6	7.0	3.0	6.4	
	HS	4.0	9.2	−0.4		

[a] This work. [b] Optimized D_3 geometries of the isolated complex. [c] Taken from the crystal structure of $[Fe(bpy)_3](PF_6)_2$.[28] [d] Data from the EXAFS spectroscopy study of aqueous $[Fe(bpy)_3]^{2+}$.[16]

The RT aqueous structure of the d^6 $[Ru(bpy)_3]^{2+}$ complex has recently been determined by Röthlisberger and co-workers from a combined QM/MM and classical MD study at RT.[29] A Ru−N bond length of 2.077 Å was obtained from their 2.9 ps QM/MM simulation. This bond length is intermediate between those found in the LS and HS structures of $[Fe(bpy)_3]^{2+}$. It also leads to an arrangement of the ligands characterized by $r(C_2-C'_2)$ = 1.468 Å, β = 78.4°, and γ = 1.5°, which is thus intermediate between the arrangements found in the LS and HS solution structures of $[Fe(bpy)_3]^{2+}$. Still, the standard deviations associated with the thermal distributions of these parameters in aqueous $[Ru(bpy)_3]^{2+}$ (Ru−N: 0.046 Å; $C_2-C'_2$: 0.021 Å; β: 1.6°; γ: 6.2°)[29] are smaller than those found for aqueous $[Fe(bpy)_3]^{2+}$. Given that the Ru−bpy bond is stronger than the Fe−bpy bond, these results suggest that, while the arrangement of the bpy ligands in a $[M(bpy)_3]^{2+}$ complex is determined by the M−N equilibrium distance, their thermal fluctuation is ruled by the strength of the M−N bond.

For characterizing the organization of the solvent around $[Fe(bpy)_3]^{2+}$ in the LS and HS states, we have calculated for both spin states the radial distribution functions (RDFs) $g(r)$ of the water oxygen (O) and hydrogen (H_w) atoms with respect to the Fe atom. They are plotted in Figure 4 with the associated running coordination number cn(r).[30]

The LS and HS $g_{FeO}(r)$ RDFs present both a broad peak with a maximum at ∼5.7 Å and a minimum at ∼6.3 Å, which defines the first solvation shell, and a second broad peak centered at ∼7.6 Å defining the second solvation shell. These features are shared by the LS and HS $g_{FeH_w}(r)$ RDFs, the first peak being however less pronounced, especially for the HS RDF. The RDFs of Figure 4 are actually similar to the $g_{RuO}(r)$ and $g_{RuH_w}(r)$ RDFs determined for aqueous $[Ru(bpy)_3]^{2+}$ from

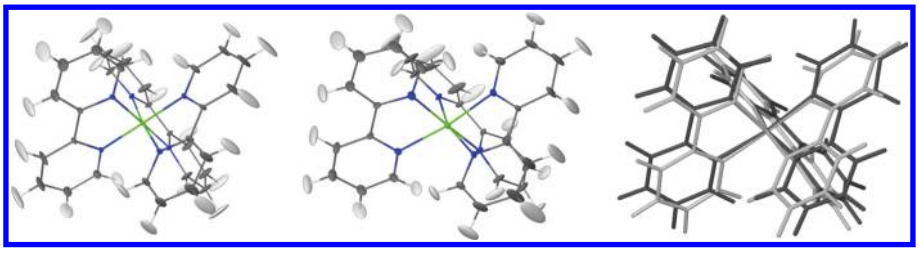

Figure 3. Average structure of aqueous $[Fe(bpy)_3]^{2+}$; views of the LS (left) and HS (center) structures showing 50 % probability ellipsoids and (right) superimposed LS (light gray) and HS (dark gray) structures.

DOI: 10.1021/jz100548m | J. Phys. Chem. Lett. 2010, 1, 1830–1835

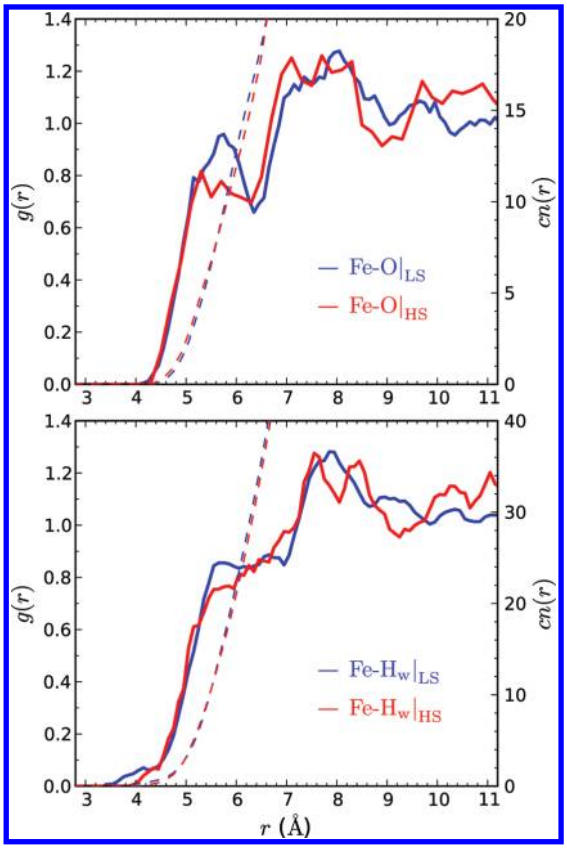

Figure 4. LS and HS RDFs $g(r)$ of the water oxygen and hydrogen atoms with respect to the Fe atom (solid lines, left y-axis) and running coordination numbers cn(r) (dashed lines, right y-axis).

a ~1 ns classical simulation.[29] Hence, the short-range order of water near a $[M(bpy)_3]^{2+}$ complex tends to be preserved upon transmetalation or a change of spin states.[32] In particular, the first solvation shell of $[M(bpy)_3]^{2+}$ consists of water molecules intercalated between the ligands (Figure 5). From the classical description of aqueous $[Ru(bpy)_3]^{2+}$, there are ~15 such water molecules. For aqueous $[Fe(bpy)_3]^{2+}$, assuming the same value of ~6.3 Å for the radius of the first solvation shell, this coordination number[33] becomes ~17 and ~15 in the LS and the HS states, respectively. About two water molecules are thus predicted to be expelled from the first solvation shell of $[Fe(bpy)_3]^{2+}$ upon SCO. This can be ascribed to a decrease of the volume accessible to the solvent in the groove between the ligands following the decrease of the depth of the groove upon the lengthening of the Fe−N bond and the increased thermal fluctuations. Note that a contribution to the changes in the RDF upon SCO from a slight expansion of the first solvation shell cannot be excluded.[34]

Figure 5 shows the plot for the two spin states of the ratio of the Fe−H_w to Fe−O running coordination number against the distance r to the Fe atom; $\eta(r) = cn_{FeH_w}(r)/cn_{FeO}(r)$. The two curves are similar to the one previously reported for aqueous $[Ru(bpy)_3]^{2+}$.[29] Thus, $\eta(r) \gg 2$ at very short distances because the smaller van der Waals radius of the H atom allows the water H atoms to get closer to the Fe atom than the O atoms (Figure 4). With increasing r, $\eta(r)$ falls below 2 because

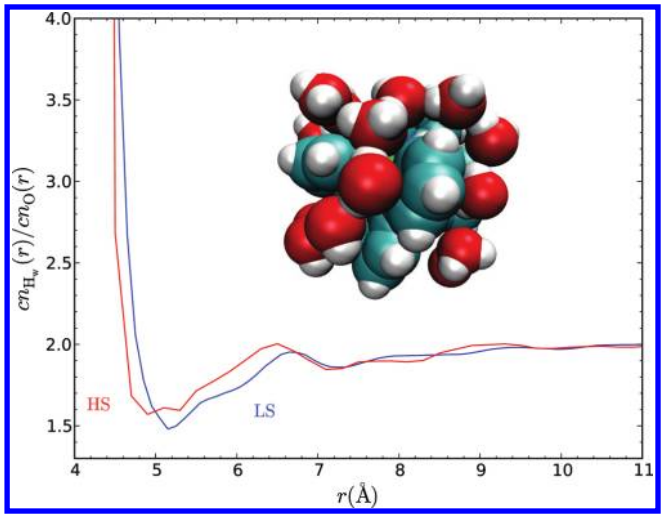

Figure 5. Plot for the LS and HS states of the ratio of the Fe−H_w to the Fe−O running coordination number against the distance r to the Fe atom illustrating the orientation of the water molecules induced by $[Fe(bpy)_3]^{2+}$. Inset: snapshot from the LS trajectory showing the first solvation shell of the complex (van der Waals representation of $[Fe(bpy)_3]^{2+}$ and water molecules with the O atoms within 6.45 Å of the Fe atoms).

of the orientation of the O atoms toward the positively charged Fe^{2+} ion and then tends toward the bulk value of 2. The value of the ratio remains however greater than 1 because the water molecules of the first solvation shell actually form a linear chain, as shown in Figure 5. Because the cutoff radius at which the probability of finding a water H atom becomes nonvanishing increases upon SCO, whereas this radius does not change for the O atoms (Figure 4); one notes in Figure 5 that the HS $\eta(r)$ curve has a shallower minimum than the LS curve and that it is also shifted toward smaller distances. That is, the reorganization of the solvation shell entailed by SCO tends to preserve the equilibrium distance between the Fe^{2+} cation and the O atoms while reorienting the water H atoms toward the bulk.

The solvation structure of the Cl^- ions has also been characterized (see SI); it remains unchanged upon the LS to HS change of states and agrees very well with those previously reported for aqueous Cl^-.[35] The analysis of the recorded trajectories shows that there is actually no pairing between the $[Fe(bpy)_3]^{2+}$ cation and the chloride anions, the average distances between the Fe atom and the Cl atoms being 10.2 and 10.9 Å, respectively (9.9 and 10.9 Å), in the LS (HS) state with standard deviations of 0.6 Å (0.3 Å).

In summary, we have been able to achieve a unique description of the structure of $[Fe(bpy)_3]^{2+}$ and its solvation shell and of its evolution upon the LS to HS SCO. Using the results reported herein as reference data, we are directing our efforts toward setting up a reliable QM/MM framework so as to investigate the mechanism of the photoinduced SCO.

SUPPORTING INFORMATION AVAILABLE Computational details; LS and HS Cl−O and Cl−H_w RDFs. The LS and HS average structures of aqueous $[Fe(bpy)_3]^{2+}$ are available as PDB files. This material is available free of charge via the Internet at http://pubs.acs.org.

DOI: 10.1021/jz100548m | J. Phys. Chem. Lett. 2010, 1, 1830–1835

AUTHOR INFORMATION

Corresponding Author:

*To whom correspondence should be addressed. E-mail: max.lawson@unige.ch.

ACKNOWLEDGMENT This work has benefited from the financial support of the Swiss National Science Foundation (Contract 200020-125175) and the MAGMANet NoE of the European Union (Contract NMP3-CT-2005-515767-2). We thank the Swiss National Supercomputing Centre (CSCS) for the calculation resources allocated under project ID 103.

REFERENCES

(1) *Spin Crossover in Transition Metal Compounds I–III*; Gütlich, P., Goodwin, H. A., Eds.; Springer-Verlag: Heidelberg, Geramany, 2004; Vol. 233–235.

(2) Hauser, A. Excited-State Lifetimes of $[Fe(bipy)_3]^{2+}$ and $[Fe(phen)_3]^{2+}$. *Chem. Phys. Lett.* **1990,** *173*, 507–512.

(3) Hauser, A. Light-Induced Spin Crossover and the High-Spin→Low-Spin Relaxation. *Top. Curr. Chem.* **2004,** *234*, 155–198.

(4) Lawson Daku, L. M.; Vargas, A.; Hauser, A.; Fouqueau, A.; Casida, M. E. Assessment of Density Functionals for the High-Spin/Low-Spin Energy Difference in the Low-Spin Iron(II)tris(2,2′-bipyridine) Complex. *ChemPhysChem* **2005,** *6*, 1393–1410.

(5) Hauser, A.; Enachescu, C.; Lawson Daku, M.; Vargas, A.; Amstutz, N. Low-Temperature Lifetimes of Metastable High-Spin States in Spin-Crossover and in Low-Spin Compounds: The Rule and Exceptions to the Rule. *Coord. Chem. Rev.* **2006,** *250*, 1642–1652.

(6) Vargas, A.; Hauser, A.; Lawson Daku, L. M. Influence of Guest–Host Interactions on the Structural, Energetic, and Mössbauer Spectroscopy Properties of Iron(II)tris(2,2′-bipyridine) in the Low-Spin and High-Spin States: A Density-Functional Theory Study of the Zeolite-Y Embedded Complex. *J. Chem. Theory Comput.* **2009,** *5*, 97–115.

(7) Monat, J. E.; McCusker, J. K. Femtosecond Excited-State Dynamics of an Iron(II) Polypyridyl Solar Cell Sensitizer Model. *J. Am. Chem. Soc.* **2000,** *122*, 4092–4097.

(8) Brady, C.; Callaghan, P. L.; Ciunik, Z.; Coates, C. G.; Døssing, A.; Hazell, A.; McGarvey, J. J.; Schenker, S.; Toftlund, H.; Trautwein, A. X.; et al. Molecular Structure and Vibrational Spectra of Spin-Crossover Complexes in Solution and Colloidal Media: Resonance Raman and Time-Resolved Resonance Raman Studies. *Inorg. Chem.* **2004,** *43*, 4289–4299.

(9) Juban, E. A.; Smeigh, A. L.; Monat, J. E.; McCusker, J. K. Ultrafast Dynamics of Ligand-Field Excited States. *Coord. Chem. Rev.* **2006,** *250*, 1783–1791.

(10) Smeigh, A. L.; Creelman, M.; Mathies, R. A.; McCusker, J. K. Femtosecond Time-Resolved Optical and Raman Spectroscopy of Photoinduced Spin Crossover: Temporal Resolution of Low-to-High Spin Optical Switching. *J. Am. Chem. Soc.* **2008,** *130*, 14105–14107.

(11) Wolf, M. M. N.; R. Gross, C. S.; Wolny, J. A.; Schünemann, V.; Døssing, A.; Paulsen, H.; McGarvey, J. J.; Diller, R. Sub-Picosecond Time Resolved Infrared Spectroscopy of High-Spin State Formation in Fe(II) Spin Crossover Complexes. *Phys. Chem. Chem. Phys.* **2008,** *10*, 4264–4273.

(12) Huse, N.; Kim, T. K.; Jamula, L.; McCusker, J. K.; de Groot, F. M. F.; Schoenlein, R. W. Photo-Induced Spin-State Conversion in Solvated Transition Metal Complexes Probed via Time-Resolved Soft X-ray Spectroscopy. *J. Am. Chem. Soc.* **2010,** *132*, 6809–6816.

(13) Gawelda, W.; Pham, V.-T.; Benfatto, M.; Zaushitsyn, Y.; Kaiser, M.; Grolimund, D.; Johnson, S. L.; Abela, R.; Hauser, A.; Bressler, C.; et al. Structural Determination of a Short-Lived Excited Iron(II) Complex by Picosecond X-Ray Absorption Spectroscopy. *Phys. Rev. Lett.* **2007,** *98*, 057401.

(14) Gawelda, W.; Pham, A. C. V.-T.; van Mourik, F.; Bressler, C.; Chergui, M. Ultrafast Nonadiabatic Dynamics of $[Fe^{II}(bpy)_3]^{2+}$ in Solution. *J. Am. Chem. Soc.* **2007,** *129*, 8199–8206.

(15) Bressler, C.; Milne, C.; Pham, V.-T.; ElNahhas, A.; van der Veen, R. M.; Gawelda, W.; Johnson, S.; Beaud, P.; Grolimund, D.; Kaiser, M.; et al. Femtosecond XANES Study of the Light-Induced Spin Crossover Dynamics in an Iron(II) Complex. *Science* **2009,** *323*, 489–492.

(16) Gawelda, W.; Pham, V.-T.; van der Veen, R. M.; Grolimund, D.; Abela, R.; Chergui, M.; Bressler, C. Structural Analysis of Ultrafast Extended X-Ray Absorption Fine Structure with Subpicometer Spatial Resolution: Application to Spin Crossover Complexes. *J. Chem. Phys.* **2009,** *130*, 124520.

(17) Consani, C.; Prémont-Schwarz, M.; ElNahhas, A.; Bressler, C.; van Mourik, F.; Cannizzo, A.; Chergui, M. Vibrational Coherences and Relaxation in the High-Spin State of Aqueous $[Fe^{II}(bpy)_3]^{2+}$. *Angew. Chem., Int. Ed.* **2009,** *48*, 7184–7187.

(18) Ando, H.; Nakao, Y.; Sato, H.; Sakak, S. Theoretical Study of Low-Spin, High-Spin, and Intermediate-Spin States of $[Fe^{III}(pap)_2]^{+}$ (pap = *N*-2-pyridylmethylidene-2-hydroxyphenylaminato). Mechanism of Light-Induced Excited Spin State Trapping. *J. Phys. Chem. A* **2007,** *111*, 5515–5522.

(19) Suaud, N.; Bonnet, M.-L.; Boilleau, C.; Labèguerie, P.; Guihéry, N. Light-Induced Excited Spin State Trapping: Ab Initio Study of the Physics at the Molecular Level. *J. Am. Chem. Soc.* **2009,** *131*, 715–722.

(20) de Graaf, C.; Sousa, C. Study of the Light-Induced Spin Crossover Process of the $[Fe^{II}(bpy)_3]^{2+}$ Complex. *Chem.—Eur. J.* **2010,** *16*, 4550–4556.

(21) The mechanism of the photoinduced SCO in iron complexes has also been the subject of recent theoretical studies,[18−20] wherein the ground- and excited-state potential energy surfaces of the isolated chromophores are characterized along this experimentally probed reaction coordinate.

(22) Car, R.; Parrinello, M. Unified Approach for Molecular Dynamics and Density-Functional Theory. *Phys. Rev. Lett.* **1985,** *55*, 2471–2474.

(23) *CPMD*, version 3.13; IBM Corp., **1990–2008** and MPI für Festkörperforschung: Stuttgart, Germany, **1997–2001**.

(24) Hutter, J.; Iannuzzi, M. CPMD: Car-Parrinello Molecular Dynamics. *Z. Kristallogr.* **2005,** 549–551.

(25) Becke, A. D. Density-Functional Exchange Energy Approximation with Correct Asymptotic Behavior. *Phys. Rev. A* **1988,** *38*, 3098–3100.

(26) Lee, C.; Yang, W.; Parr, R. G. Development of the Colle–Salvetti Correlation-Energy Formula into a Functional of the Electron Density. *Phys. Rev. B* **1988,** *37*, 785–789.

(27) The AIMD study of such a large system is computationally demanding, especially in the HS state, wherein, owing to the fact that the calculations are run unrestricted, we come close to the hardware limitations (memory requirements and computations dominated by communications).

(28) Dick, S. Crystal Structure of Tris(2,2′-bipyridine)iron(II) Bis(hexafluorophosphate), $(C_{10}H_8N_2)_3Fe(PF_6)_2$. *Z. Kristallogr. New Cryst. Struct.* **1998,** *213*, 356.

(29) Moret, M.-E.; Tavernelli, I.; Röthlisberger, U. Combined QM/MM and Classical Molecular Dynamics Study of $[Ru(bpy)_3]^{2+}$ in Water. *J. Phys. Chem. B* **2009,** *113*, 7737–7744.

DOI: 10.1021/jz100548m | *J. Phys. Chem. Lett.* **2010,** *1*, 1830–1835

(30) A radial grid of 0.1 Å was used for the calculations of the RDFs, except for $Fe-O|_{HS}$, for which a grid of 0.2 Å was used.
(31) Vargas, A.; Zerara, M.; Krausz, E.; Hauser, A.; Lawson Daku, L. M. Density-Functional Investigation of the Geometric, Energetic and Optical Properties of the Cobalt(II)tris(2,2′-bipyridine) Complex in the High-Spin and in the Jahn−Teller Unstable Low-Spin States. *J. Chem. Theory Comput.* **2006,** *2*, 1342–1359.
(32) Note however that the picture obtained here for the structure of water around a $[M(bpy)_3]^{2+}$ complex is likely to evolve in the presence of phenomena such as a Jahn−Teller instability, as in the case[31] of the LS $[Co(bpy)_3]^{2+}$ complex.
(33) The coordination number is the value of the running coordination number cn(r) at the radius of the first solvation shell, which is given by the minimum of the RDF after the first peak.
(34) For an accurate comparison of the LS and HS coordination numbers, the RDFs should be calculated with the same radial grid because the coordination number is sensitive to the determination of the radius of the first solvation shell. Using for the calculation of the HS Fe−O RDF the same 0.1 Å radial grid as that for the LS Fe−O RDF, the radius determined for the first solvation shell in the HS state remains unchanged at ∼6.3 Å. However, the calculated HS RDF becomes noisier because of the small simulation time accessible for the HS state. The larger simulation times accessible within a QM/MM approach for both spin states will allow us to increase the resolution of the RDFs, thus making their comparison more accurate.
(35) Heuft, J. M.; Meijer, E. J. Density Functional Theory Based Molecular-Dynamics Study of Aqueous Chloride Solvation. *J. Chem. Phys.* **2003,** *119*, 11788–11791.

DOI: 10.1021/jz100548m | *J. Phys. Chem. Lett.* **2010,** *1*, 1830–1835